Polymer 210 (2020) 122959

Contents lists available at ScienceDirect

Polymer

journal homepage: http://www.elsevier.com/locate/polymer

Following isothermal and non-isothermal crystallization of poly (3-hexylthiophene) thin films by UV–vis spectroscopy

Mina Alizadehaghdam [a], Barbara Heck [b], Silvia Siegenführ [b], Yaser A. AlShetwi [b,c], Fanuel M. Keheze [b], Sebastian Stäter [d], Farhang Abbasi [a,*], Günter Reiter [b,**]

[a] Institute of Polymeric Materials and Faculty of Polymer Engineering, Sahand University of Technology, New Town of Sahand, Tabriz, Iran
[b] Physikalisches Institut, Albert-Ludwigs-Universität Freiburg, Hermann-Herder-Straße 3, 79104, Freiburg, Germany
[c] Materials Science Research Institute, King Abdulaziz City for Science and Technology (KACST), Riyadh, Saudi Arabia
[d] Zernike Institute for Advanced Materials, University of Groningen, Nijenborgh 4, 9747, AG Groningen, Netherlands

ARTICLE INFO

Keywords:
Poly(3-hexylthiophene)
UV–vis absorption spectra
Isothermal crystallization
Non-isothermal crystallization
Franck-Condon relation

ABSTRACT

We investigated non-isothermal and isothermal crystallization of spin-coated poly(3-hexylthiophene) thin films prepared from the melt by *in-situ* ultraviolet–visible absorption spectroscopy. Analyzing the absorption spectra according to the Franck-Condon principle allowed for a quantitative assessment of the degree of crystallinity as well as the quality of order within crystalline regions of the films. Measured at room temperature, we observed a similar crystallinity for all differently crystallized films. The highest quality of order, however, was found for the P3HT film cooled slowly from the melt. These results were in full agreement with the results obtained by X-ray diffraction and calorimetry measurements. Consistently, in spite of similar crystallinities, atomic force microscopy images did not show a well-defined structure of ordered domains of preferentially aligned lamellae for the films rapidly cooled from the melt. In addition, heating the P3HT films in a specific range of temperature showed no change in crystallinity in spite of a continuous loss of order quality. Our results revealed that crystallinity and crystalline quality could behave differently while processing a semicrystalline polymer.

1. Introduction

Poly(3-alkylthiophene)s (P3ATs) have become a model system for the research on conjugated polymers, in terms of both fundamental and application-oriented studies [1]. In particular, regioregular poly (3-hexylthiophene) (rr-P3HT) has emerged as a key material for the elaboration of organic field effect transistors (OFETs) and organic solar cells (OSCs) due to the combination of its facile processability, large charge carrier mobility and environmental stability [2–10]. Charge transport is a complex multiscale process, extremely sensitive to the intra- and interchain order in these semiconducting polymers [2]. Hence, there is a continuous effort to improve the degree of order in the conjugated polymers, which is examined through different techniques such as small angle X-ray scattering (SAXS) and wide angle X-ray scattering (WAXS) [11–14], nuclear magnetic resonance (NMR) [15,16], atomic force microscopy (AFM) [17], transmission electron microscopy (TEM) [18], differential scanning calorimetry (DSC) [19], infrared (IR) spectroscopy [16], and ultraviolet–visible (UV–vis) spectroscopy [20,21].

UV–vis spectroscopy is a technique which is used to measure the absorption of radiation in UV–vis range, as a function of wavelength, when interacting with a material. rr-P3HT can form ordered aggregates in solution or in the solid state, for example in thin films. The absorption spectrum of P3HT thin films can be interpreted using a weakly interacting H-aggregate model, providing quantitative estimates not only of the fraction of the film made up of aggregates (*i.e.* crystallinity of the film), but also the degree of excitonic coupling (*i.e.* crystalline quality) within the aggregates [22].

Many investigations have applied UV–vis absorption spectroscopy to study the improvement of overall (intra- and interchain) order in the P3HT aggregates prepared from solution following different approaches such as changing the solvent quality [16,22,23], using mixed solvents [20,24–26], sonicating [27,28], aging [28] or when changing regioregularity [29] and molecular weight of the polymer [26]. In a work done by Roehling et al. [23], P3HT crystallization in solution was controlled using various solvents and the resulting changes in microstructure were

* Corresponding author.
** Corresponding author.
E-mail addresses: f.abbasi@sut.ac.ir (F. Abbasi), guenter.reiter@physik.uni-freiburg.de (G. Reiter).

https://doi.org/10.1016/j.polymer.2020.122959
Received 27 June 2020; Received in revised form 12 August 2020; Accepted 15 August 2020
Available online 29 August 2020
0032-3861/

attributed to three separate causes: the fractionation of polymer chains due to solubility differences, differences in chain conformations induced by interactions with solvent molecules, and the kinetics of structure formation. When improving the solvent quality, the $A_{0\text{-}0}/A_{0\text{-}1}$ peak ratio in the absorption spectra became larger, suggesting a lower free exciton bandwidth, an increasing intrachain order and longer conjugation lengths. X-ray diffraction (XRD) data revealed the same trend of increasing and correlated intra- and interchain order with improving solvent quality. In another quantitative work by Scharsich et al. [26], the absorption spectra were analyzed according to the Franck-Condon principle. They revealed that adding a poor solvent to the low molecular weight P3HT dissolved in a good solvent enhanced the intensity of the $A_{0\text{-}0}$ peak. However, for long P3HT chains, this intensity increased only when small amounts of poor solvent were added but decreased for higher fractions of the poor solvent. Choi et al. [25] showed that ultrasonication facilitated formation of rod-like nanostructures of P3HT in solution, enhancing intra- and intermolecular interactions among P3HT chains. Increasing the molecular weight and the regioregularity of the polymer led to an increase of absorption at the lowest energy ($A_{0\text{-}0}$) and to an increased intrachain order as deduced from an analysis of the UV–vis spectra [26,30].

Works employing UV–vis spectroscopy to study P3HT crystallinity in the solid state, usually focused on the improvement of crystalline order in P3HT thin films caused by some post-treatment processes such as high-temperature rubbing. Hamidi-Sakr et al. [30] succeeded to increase the ratio $A_{0\text{-}0}/A_{0\text{-}1}$ and the overall crystallinity of P3HT in thin films via a high temperature rubbing procedure. Increasing the rubbing temperature resulted in better-ordered P3HT chains in the thin films. To sum up, varying processing conditions have been applied vastly to control crystallization of P3HT from the solution. However, such a systematic study of P3HT crystallization starting from the melt by a thorough analysis of the corresponding *in-situ* UV–vis spectra is missing in the literature. This prevents a revealing comparison to be provided between P3HT crystals prepared from the solution and those obtained from the melt.

In our previous works [31,32] employing mainly calorimetry assessments, we focused on disputes over reliable values for thermodynamic properties of P3HT crystals, *i.e.* equilibrium melting temperature and enthalpy of fusion of an ideal P3HT crystal. In the present work, however, we have focused on how the kinetics of crystallization and different crystallization conditions affect crystallinity and crystalline quality (*i.e.* quality of order within the crystalline regions) of the samples, using mainly UV–vis spectroscopy assessments along with a Franck-Condon analysis. Differences in the generated nanostructures were also evaluated by AFM studies, combined with DSC and X-ray scattering analyses on similarly crystallized bulk P3HT samples to support and complement our findings deduced from UV–vis absorption measurements. Finally, a few AFM phase images from the P3HT crystals prepared from the solution provided a preliminary step for a thorough comparing study between the solution- and melt-grown P3HT crystals in a future work.

2. Experimental details

2.1. Materials

Poly(3-hexylthiophene) (P3HT) was obtained from Merck Chemicals (Germany). The number average molecular weight, $\overline{M}_n = 19$ kg/mol and dispersity, $Đ = 1.67$ were measured by gel permeation chromatography (GPC). The regioregularity of P3HT (= 93%) was determined using proton nuclear magnetic resonance (^{1}H NMR).

2.2. UV–vis absorption spectroscopy

P3HT was dissolved in chloroform at a concentration of 20 mg/ml and kept in an oil bath at 60 °C for 1 h. Films of a thickness of *ca.* 200 nm (measured by AFM) were made by spin-coating of the obtained solution onto glass substrates, cleaned previously in an ultrasonic bath containing ethanol at 50 °C for 15 min. The spinning speed and time were 1000 rpm and 60 s, respectively. The prepared films are called “as-cast” in Appendix A (Tables 1 and 3) and in Fig. 6. First, to erase memory effects, films were brought to 260 °C and kept there for 1 min, in a hot stage purged with nitrogen (Linkam Scientific Instruments, UK) and controlling the temperature to a precision of about 0.1 °C. The sample was subsequently taken at a cooling rate of 100 °C/min to a chosen temperature T_c where it remained for 4 h to crystallize the polymer. Afterwards, the sample was quenched to room temperature (at the rate of 100 °C/min). Employing several samples, the value of T_c was varied from 150 to 225 °C. These crystallized films were named correspondingly (T_c150, …, T_c225) in Appendix A (Table 1) and in Fig. 6. In addition, complementary samples were prepared by cooling them slowly (1 °C/min) and rapidly (100 °C/min) from the molten state at 260 °C to the room temperature, labeled “slowly cooled” and “rapidly cooled”, respectively, in this work.

To identify contributions from ordered and disordered regions within the sample, UV–vis absorption spectra for the crystallized P3HT films were recorded over areas with a diameter of *ca.* 40 μm using a Zeiss Axio 100 microscope connected to a spectrometer (Ocean Optics USB 2000) via an optical fiber of 400 μm in diameter. A halogen lamp was used as the light source and the spectra were collected in the transmission mode, using a 10x objective lens.

2.3. Atomic force microscopy (AFM)

AFM measurements on the samples prepared for UV–vis absorption spectroscopy were performed with a JPK BioMAT™ setup, consisting of a NanoWizard® AFM, the BioMAT™ base and a Zeiss Axio Imager optical microscope. AFM images were obtained in the tapping mode at ambient conditions. AFM cantilevers made of silicon (type: PPP-NCL-W) were purchased from Nanosensors®. The Si-tips used had a resonance frequency of about 180 kHz and a spring constant of about 30 N/m.

2.4. Differential scanning calorimetry (DSC)

Semi-crystalline P3HT samples were prepared using a differential scanning calorimeter (DSC), Perkin-Elmer Model DSC4, operated under a nitrogen atmosphere. 4 (±0.1) mg of the polymer was introduced into a DSC pan. The pan was sealed and heated up to 260 °C (well above the nominal melting temperature of P3HT around 240 °C), at a heating rate of 20 °C/min. The sample was kept at 260 °C for 1 min to assure complete melting of the polymer and to erase memory effects. After the sample had reached the temperature T_c at the maximum possible cooling rate accessible with the DSC apparatus (200 °C/min), it was kept at T_c for 4 h to crystallize the polymer. Afterwards, the sample was quenched to room temperature (at a rate of 200 °C/min). The temperature was then raised at a rate of 20 °C/min to record the peak of the melting curve identified as the melting temperature (T_m) and the area under this peak as the enthalpy of fusion (ΔH_m). The value of T_c was varied from 150 to 216 °C. In addition, two samples were prepared by cooling them slowly (1 °C/min) and rapidly (200 °C/min) from the molten state at 260 °C, labeled “slowly cooled” and “rapidly cooled”, respectively (Fig. 6 and Appendix E (Table 4)). The T_m and ΔH_m values reported in Fig. 5 were recorded by heating the samples after 4 h isothermal crystallization to the melting point directly (*i.e.* the samples were not quenched to room temperature before heating). To identify a baseline and to subtract it from the DSC curves, a heating run from 25 to 260 °C at a rate of 20 °C/min was performed with an empty sealed DSC pan.

2.5. Small/wide-angle X-ray scattering (SAXS/WAXS)

To provide samples for SAXS/WAXS measurements, P3HT was

crystallized in the DSC apparatus similar to the samples prepared for DSC measurements. Pans were opened and the crystallized samples of P3HT were taken out. In order to accomplish random orientations, these samples were divided into small pieces with a sharp blade and then transferred to a sample holder for SAXS/WAXS measurements. The overall sample mass was about 12 mg.

The SAXS experiments were carried out at room temperature with the aid of a Kratky-camera attached to a conventional Cu-Kα X-ray source having a wavelength λ = 0.1542 nm. The scattering vector is s = 2sinθ/λ, with the scattering angle θ. Scattering curves were registered using a position-sensitive metal wire detector. The obtained slit-smeared data were deconvoluted using an algorithm developed by Strobl. [33] During the measurements, the sample chamber was under vacuum.

WAXS measurements were performed at room temperature in the reflection mode using a modified Siemens D500 X-ray diffractometer with a conventional Cu-Kα X-ray source at a wavelength λ = 0.1542 nm.

2.6. Preparing P3HT nanofibers from the solution

P3HT was dissolved in 3-hexylthiophene at a concentration of 0.2 mg/ml in a vial at 100 °C for 30 min. Then the vial was transferred to room temperature and nanofibers were formed upon reducing the solution temperature, as the color of the solution turned from yellowish brown to purple. In addition, P3HT was dissolved in toluene at a concentration of 5 mg/ml in a vial at 80 °C for 30 min. Then the vial was kept in the darkness at room temperature for 1 week to encourage gradual formation of the nanofibers. Finally, the solution was diluted to 0.5 mg/ml. The suspended nanofibers were spin coated on the silicon substrates for the following evaluations with atomic force microscopy.

3. Results and discussion

3.1. Crystalline features of P3HT films deduced from the analysis of UV–vis absorption spectra

3.1.1. Determination of crystalline contribution in the absorption spectra

Applying the Franck-Condon principle, UV–vis absorption spectra of a crystallized P3HT film can be interpreted as a superposition of two distinct contributions representing two different states of molecular order. The low-energy absorbance vibronic peaks are attributed to chains in crystalline states, that is, π-stacked chains forming weakly interacting H-aggregates. The remaining high-energy contribution to the spectrum arises from intra-chain states of coiled (amorphous) chains [20–22,26,34,35]. The fraction of the spectrum attributed to absorption from aggregates is determined using a modified Franck-Condon fit (equation (1)) developed by Spano and co-workers [22]:

$$A(E) \propto \sum_{m=0} \left(\frac{e^{-S} S^m}{m!} \right) \left(1 - \frac{We^{-S}}{2E_P} \sum_{n \neq m} \frac{S^n}{n!(n-m)} \right)^2 \exp\left[- \frac{(E - E_0 - mE_P)^2}{2\sigma^2} \right] \quad (1)$$

where $A(E)$ is the intensity of absorption, S is the Huang-Rhys parameter of disordered chains ($S = 1.1$) [35], E_P is the vibrational energy of the effective carbon-stretching mode ($E_P = 175$ meV) [20,35]. The parameters remaining free for fitting are m, the vibrational level, W, the free exciton bandwidth, E_0, the transition energy of the lowest energy peak $A_{0\text{-}0}$, and σ, the width of the Gaussian line shape functions. The summation $\sum_{n \neq m} \ldots$ is over the vibrational quantum number n [21]. For simplicity, a single Gaussian line shape is used with the same width (σ) for each vibronic transition, introduced in the exponential term of the equation [22].

Fig. 1 (a) presents the absorption spectrum of the P3HT film crystallized by slowly cooling (1 °C/min) the sample from the melt at 260 °C to room temperature (circles). The low-energy part of the spectrum could be fitted with three dotted (m = 2) Gaussian peaks, starting with the lowest energy peak, $A_{0\text{-}0}$, at 2.07 eV and a peak spacing of 0.175 eV. The relative area of the fitting curve (solid curve) to the total area of the experimental spectrum is related to the absorbance resulting from aggregated chains (A_c). However, due to a possible difference in the extinction coefficient of amorphous and aggregated chains, A_c cannot be directly interpreted as the fraction of aggregated chains (or as crystallinity, x_c). As the oscillator strength of aggregated chains is about 1.39 times the oscillator strength of the amorphous chains, x_c can be found through A_c/1.39 [20,22]. Absorption spectra for differently crystallized P3HT samples were analyzed along these lines and the quantitative results are presented in Appendix A (Tables 1 and 2).

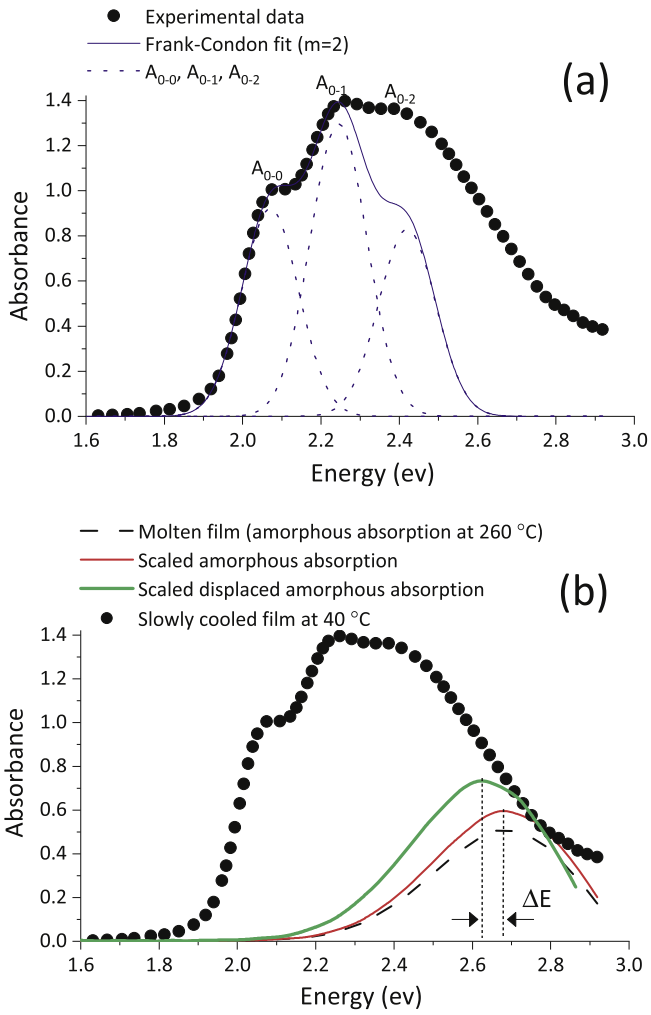

Fig. 1. (a) Absorbance spectrum taken on a P3HT film crystallized by cooling slowly (1 °C/min) from the melt at 260 °C to room temperature (circles). The solid curve shows the modified Franck-Condon fit to the spectrum consisting of three peaks (m = 2), represented each by dotted curves, $A_{0\text{-}0}$, $A_{0\text{-}1}$ and $A_{0\text{-}2}$ at 2.07, 2.24 and 2.42 eV, respectively (the peaks are spaced by 0.175 eV). See Appendix A (Table 1) for additional quantitative results of the fitting. (b) Absorbance spectrum taken on a P3HT film molten at 260 °C (dashed curve) then crystallized by cooling slowly (1 °C/min) from the melt to 40 °C (circles). The thin (red) solid curve presents the absorbance spectrum of the molten film scaled to the high-energy tail of the absorbance spectrum of the slowly cooled film. The thick (green) solid curve presents the absorbance spectrum of the molten film displaced to lower energies, as much as ΔE, then scaled to the high-energy tail of the absorbance spectrum of the slowly cooled film. (For interpretation of the references to color in this figure legend, the reader is referred to the Web version of this article.)

Another approach to extract the crystalline contribution is based on a subtraction of the amorphous contribution from the experimental absorption spectrum [20,21,26] by using the absorption spectrum of a

molten P3HT film at 260 °C (dashed curve in Fig. 1 (b)). To implement such a procedure, a molten film was crystallized by cooling slowly from 260 to 40 °C and the corresponding spectrum was then recorded at 40 °C (circles). Although a molten P3HT film is totally amorphous, its absorption spectrum cannot be considered directly as the amorphous contribution of the spectrum of the slowly cooled film at 40 °C as the absorption of amorphous P3HT at 260 °C would not be the same as that at 40 °C.

As shown in Appendix B (Fig. 9), with increasing temperature, the intensity absorbed by an amorphous (molten) P3HT becomes reduced and the position of the maximum of the peak moves towards higher energies. Therefore, to estimate the absorption of fully amorphous P3HT at 40 °C, we need to account for the changes in the spectrum with temperature and to shift the spectrum of the molten P3HT measured at 260 °C (dashed curve in Fig. 1 (b)) by ΔE to a lower energy. In addition, we have to increase the absorbance. The shift of the peak position of amorphous P3HT was assumed to follow a linear functionality of temperature according to the equation extracted from the measured data shown in Appendix B (Fig. 9), yielding the value of ΔE (which was used in Fig. 1 (b)) by extrapolation to 40 °C. The amount of increase in the intensity was derived by scaling to the high-energy tail of the absorption spectrum of the slowly cooled P3HT film (thick solid line in Fig. 1 (b)). From Fig. 1 (b) and Appendix A (Table 3), scaling the molten spectrum without shifting in the energy axis (thin solid line), as applied in previous studies [20,21,26], may cause an underestimation of the amorphous contribution by as much as *ca.* 6%. The values of the crystallinity obtained by subtracting the shifted and scaled molten spectrum from the absorption spectra of the samples were also found in good agreement with the values obtained by Franck-Condon analysis.

3.1.2. *Monitoring the progress of non-isothermal crystallization with time*

In Fig. 2, we show the absorption spectra recorded for an as-cast P3HT film during the heating to the complete melting (at 260 °C) and subsequent slow (1 °C/min) or rapid (40 °C/min) cooling to 40 °C. During heating, the absorbance decreased continuously. The lower-energy crystalline contribution (associated with the vibronic peaks of $A_{0\text{-}0}$ and $A_{0\text{-}1}$) disappeared completely at the melting point at *ca.* 255 °C and only the higher-energy amorphous contribution survived. The decrease in absorbance with increasing temperature was most pronounced between 235 and 245 °C, *i.e.*, in the temperature range where most of the crystalline structures melted. Upon subsequent slow cooling, absorbance re-increased with a jump and the reappearance of the lower-energy vibronic features attributed to crystallization in the range from 220 to 214 °C. For a higher cooling rate, we expect crystallization to set in at a lower temperature range as confirmed in Fig. 2 (c). Cooling the sample at a rate of 40 °C/min, the jump in absorbance occurred in a lower temperature range from 210 to 200 °C.

While the shape of the spectra of the films either slowly or rapidly cooled back to 40 °C (Fig. 2 (b) and (c)) were similar to the initial spectrum of the as-cast film at 40 °C (Fig. 2 (a)), the values of the absorbance were lower. This is probably due to spreading the film during its initial melting which resulted in some reduction in the film thickness.

To have a deeper insight into the structural changes in the P3HT film caused by temperature change, we fitted the modified Franck-Condon equation (equation (1)) to all the absorption spectra presented in Fig. 2 and obtained values for the crystallinity (x_c) and the fitting parameters of W, σ and E_0. As demonstrated in Fig. 3, all fitting parameters increased when increasing the temperature from 40 to 235 °C (the free exciton bandwidth, W, from 87 to 129 meV, the disorder parameter, σ, from 77 to 92 meV and the transition energy of the lowest energy peak $A_{0\text{-}0}$, E_0, from 2.072 to 2.129 eV), expressing an increasing structural disorder. In the study by Keheze et al. [21], melting and recrystallization of a bulky substituted poly(3-(2,5-dioctylphenyl)thiophene) (PDOPT) was followed in a similar way by absorption spectroscopy. The increase in W and E_0 was explained by a gradual loss of chain planarity and

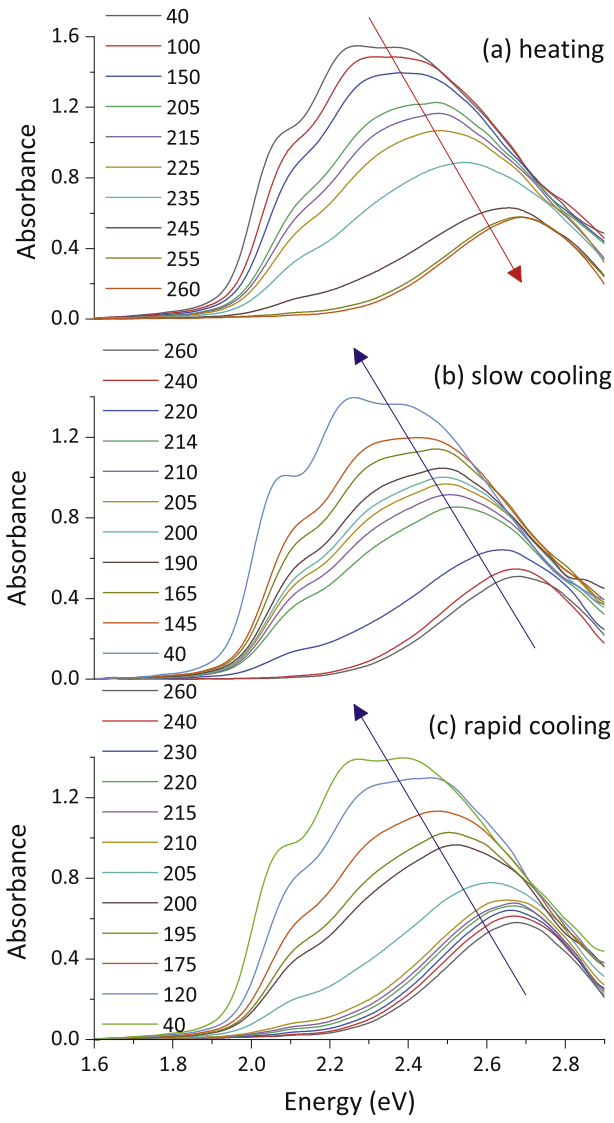

Fig. 2. Absorbance spectra taken on as-cast P3HT films heated from 40 °C up to the molten state at 260 °C with the rate of 20 °C/min (a), then cooled down to 40 °C slowly with the rate of 1 °C/min (b) or rapidly at a rate of 40 °C/min (c). The numbers show the temperatures at which the spectra were taken. The arrows are associated with the temperature increase in part (a) and the temperature decrease in parts (b) and (c). The spectra are not normalized, hence differences in the absorbance values in three parts of the figure, could be attributed to differences in the film thicknesses.

increasing intrachain disorder within an aggregate which caused the exciton to be localized. This, in turn, increased the excitonic coupling and led to higher values of W [23]. σ, associated with intercrystallite disorder, was also found to increase by heating. In good agreement with Fig. 2 (a), the increase of free exciton bandwidth and disorder parameter by heating became more pronounced in the temperature range (melting range) from 235 up to 245 °C. E_0, however, was observed to be nearly constant up to 235 °C.

In spite of the continuous increase of structural disorder, the fraction of aggregated chains (x_c) was almost unchanged up to 175 °C. This means that while the crystallinity (x_c) was constant, quality of the order decreased within the crystalline regions of the samples (*i.e.* within the aggregates), as demonstrated by the increase of the value of W. Above 175 °C, x_c started to decrease and dropped strongly above 235 °C.

After complete melting of the as-cast P3HT film at 260 °C, the molten films were crystallized at two different cooling rates, *i.e.*, slowly at 1 °C/

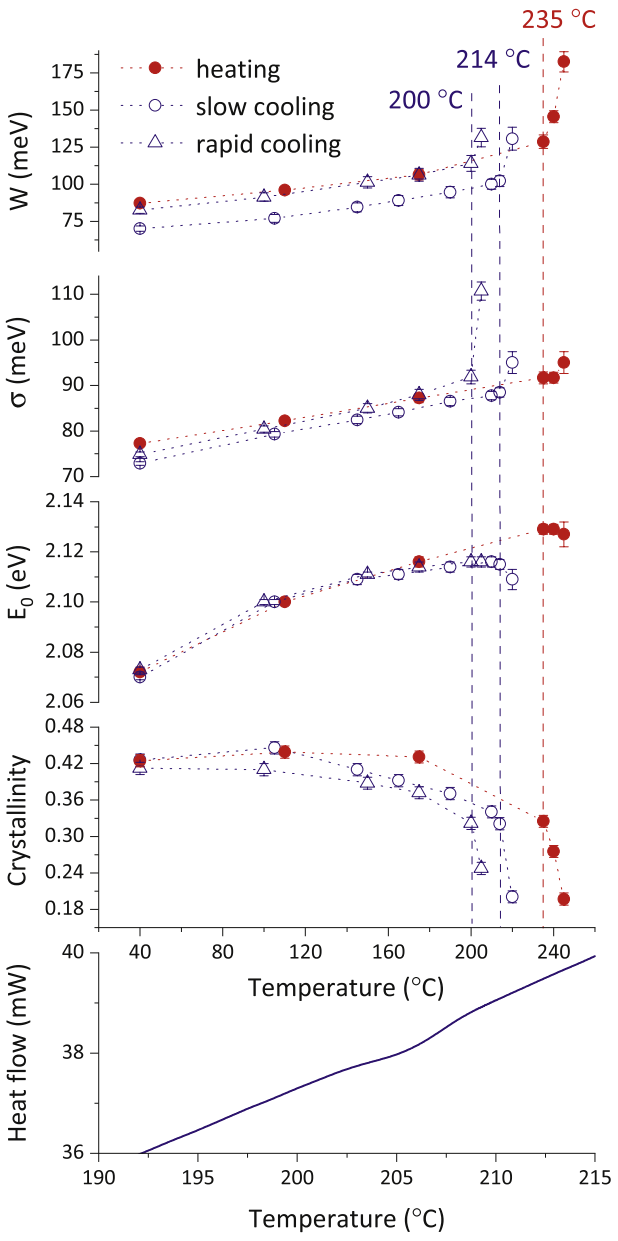

Fig. 3. Values of the free exciton bandwidth (W), the width of the Gaussian line shape function (σ), the transition energy of the lowest energy peak $A_{0\text{-}0}$ (E_0) and crystallinity (x_c), all deduced from fitting the absorption spectra presented in Fig. 2 with the Franck-Condon equation (m = 2), plotted versus temperature. The vertical dashed lines at 235, 214 and 200 °C specify the slope change in the curves associated with the heating (solid circles), slow cooling (open circles) and rapid cooling (open triangles) process, respectively. The plot in the bottom is a part of the DSC curve for cooling of a 4-mg P3HT sample slowly (1 °C/min) from the melt at 260 °C to room temperature showing the crystallization exotherm.

min or rapidly at 40 °C/min. By slow cooling, a significant drop of W and σ along with a jump in x_c were observed when the temperature was reduced below 214 °C (Fig. 3), attributed to crystallization of the film, also found from Fig. 2 (b). Further cooling the P3HT film from 214 to 40 °C led to a gentle decrease in the values of the fitting parameters of W, σ, E_0 and a gentle increase in crystallinity. In Fig. 3, the slope change in the variation of these parameters with temperature is indicated by the vertical dashed lines at 214 and 200 °C for the slowly and rapidly cooled P3HT films, respectively.

Within the whole of the temperature range, the values of exciton bandwidth (W) were lower (quality of the order was higher) for the crystallization by slow cooling compared to the crystallization by rapid cooling. However, interestingly, both slowly and rapidly cooled samples finally get similar crystallinities. This observation highlights that we have to distinguish between the crystallinity and the quality of order within crystalline domains.

The bottom plot in Fig. 3 is related to the DSC curve of a P3HT sample being cooled slowly (1 °C/min) from the melt state. The transition shown in the curve suggests that the crystallization starts from a temperature lower than 214 °C. However, it is found from the upper curves that the crystallization occurs mainly before this temperature is reached during the cooling. We believe, this discrepancy is related to the different sample preparation methods. UV–vis spectra were taken from the spin-coated P3HT films (with a mass in order of a few μg) while DSC is done for a bulk P3HT sample of about 4 mg. The nucleation process in a thin film of polymer, affected by the substrate surface, is thought to be more efficient than that in a bulk sample of polymer, making the crystallization process to be started earlier.

3.1.3. *Monitoring the progress of isothermal crystallization with time*

Fig. 4 presents the absorption spectra during the isothermal crystallization of P3HT films at different crystallization temperatures of 170, 216 and 225 °C. The absorbance jumped during a rapid cooling from the melt to T_c = 170 °C, compared to a much smaller increase in absorbance during the rapid cooling form the melt to T_c = 216 or 225 °C. Thus, crystallizing upon cooling to 170 °C the film was already largely crystalline when reaching 170 °C. Therefore, no further significant changes in absorbance were observed when the sample was kept at this temperature for 240 min.

At T_c = 216 °C, most of the isothermal crystallization occurred within the initial 5 min, followed by small increase in absorbance for the subsequent 4 h. At T_c = 225 °C, crystallization was rather slow, so that during the crystallization time of 240 min, crystallization progressed continuously. Quenching the samples to room temperature, after 240 min of isothermal crystallization at a given T_c, developed more crystallinity in the samples, evident from the increased absorbance and pronounced vibronic $A_{0\text{-}0}$ and $A_{0\text{-}1}$ peaks (dashed curves in Figure (4); see also Figure (10) in Appendix C).

Fig. 5 demonstrates how the crystallinity and crystalline quality changed with increasing isothermal crystallization time from 5 to 240 min at different T_cs. Within error bars, no improvement was observed in the intrachain order (W) at a given T_c when increasing the crystallization time. However, the intercrystallite disorder (σ) decreased from 93 to 90 and 110 to 90 meV by extending the crystallization time from 5 to 240 min for T_c = 216 °C and T_c = 225 °C, respectively. The crystallinity was nearly unchanged with the time at T_c = 170 °C as the crystallization was already about to complete in the course of cooling from the melt to T_c = 170 °C. After crystallization for 30 min at T_c = 216 °C, an almost constant value of the crystallinity was obtained. The crystallization rate at T_c = 225 °C was so slow that the crystallinity progressed continuously during 240 min of crystallization. The fusion enthalpy and melting temperature did not change measurably with the time when the film was kept at T_c = 170 °C. However, both values increased noticeably with the time at T_c = 216 °C. In spite of observing crystallization-induced changes in P3HT films in the absorption assessments taken at T_c = 225 °C, we did not succeed to crystallize the 4 mg bulk P3HT samples used for DSC experiments even after 240 min at T_c = 225 °C. Hence, no melting temperature or fusion enthalpy could be recorded by DSC for samples kept at 225 °C.

After 240 min of crystallization at T_c, the sample crystallized at a low T_c (170 °C) had higher crystallinity, but lower crystalline quality (less intrachain order within the aggregates, deduced from higher W) than the sample crystallized at a high T_c (225 °C) (Fig. 5). These results are consistent with the higher enthalpy of fusion (caused by the larger crystallization rate), but lower melting temperature (caused by the formation of thinner crystals) recorded for the sample crystallized at

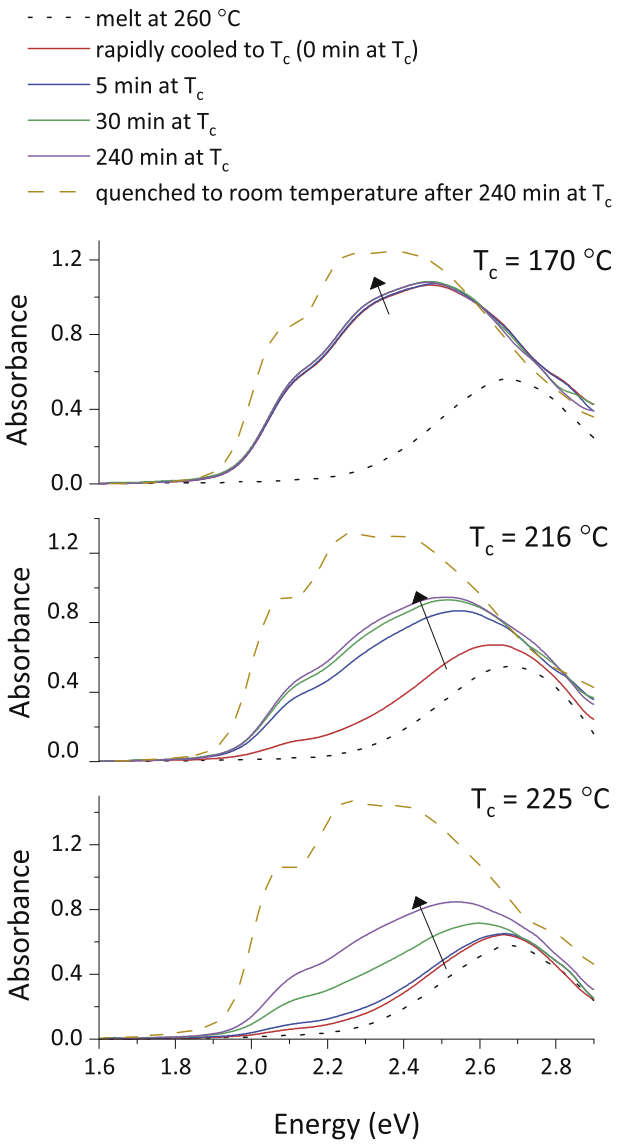

Fig. 4. Absorbance spectra taken on the as-cast P3HT films isothermally crystallized from the melt at different crystallization temperatures of $T_c = 170$, 216, and 225 °C. First, the as-cast films were molten at 260 °C (dotted curves). Subsequently, the films were rapidly cooled down to a crystallization temperature (T_c) and kept there for 4 h, with spectra taken after 0, 5, 30 and 240 min (solid curves). The arrows indicate the direction of increasing with crystallization time at each T_c. Finally, the films were quenched to room temperature (dashed curves).

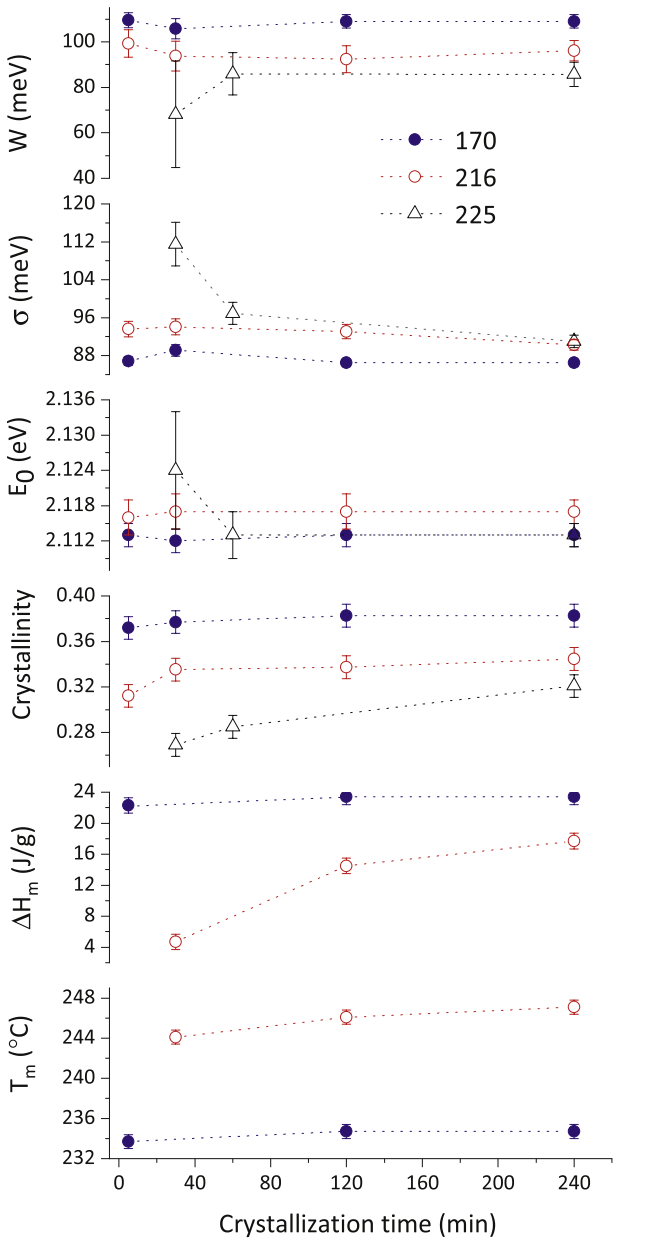

Fig. 5. The free exciton bandwidth (W), the width of the Gaussian line shape functions (σ), the transition energy of the lowest energy peak $A_{0\text{-}0}$ (E_0) and crystallinity (x_c) (all deduced from fitting the Franck-Condon equation (m = 2) to the absorption spectra, recorded at T_c), the enthalpy of fusion and melting temperature plotted versus the crystallization time for the samples isothermally crystallized from the melt at crystallization temperatures of 170 °C (solid circles), 216 °C (open circles) and 225 °C (open triangles). The enthalpy of fusion and the melting temperature were evaluated for the bulk P3HT samples with a mass of 4 mg, while the other quantities were obtained by UV–vis spectroscopy of the spin-coated P3HT films having a mass on order of a few μg.

170 °C. Polydispersity of our P3HT material could cause ΔH_m (or crystallinity) to decrease for increasing T_c. With increasing temperature, crystals require longer chains in order to be stable, and thus an increasing amount of shorter chains is not able to crystallize hence locate in the amorphous regions [36]. However, at higher crystallization temperatures, the rate of polymer crystallization is slower, providing more time for those longer polymer chains to get improved order at the crystal growth front. Intercrystallite disorder (σ) was larger for the P3HT film crystallized at $T_c = 225$ °C which might be due to its lower crystallinity, *i.e.* due to larger amorphous domains between the crystalline aggregates.

Appendix C (Fig. 10) compares the crystalline features of the samples at T_c with the corresponding values obtained after subsequent quenching to room temperature. The visible decrease in the values of the fitting parameters W, σ and E_0 determined at T_c relative to those determined at room temperature suggests that quenching the films following their isothermal crystallization has increased the crystalline quality of the samples. This could be due to some segmental motions within the crystalline domains at T_c, which are frozen in at room temperature. Increase in crystallinity and enthalpy of fusion states that the crystallization was not completed at T_c after 240 min. Thus, the samples crystallized additionally during quenching to room temperature. Quenching the samples, however, did not influence the melting temperature (the peak of melting transition in DSC curve) for each sample crystallized at T_c (Appendix C (Fig. 11)). This means that the improvement of quality of order within the crystalline regions (plus some smaller crystals),

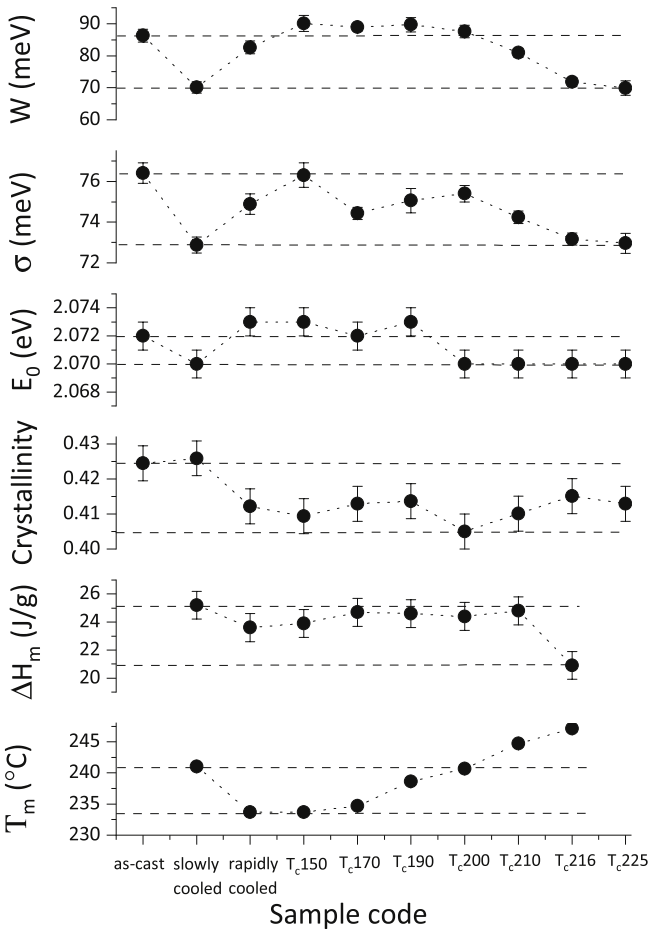

Fig. 6. The free exciton bandwidth (W), the width of the Gaussian line shape functions (σ), the transition energy of the lowest energy peak $A_{0\text{-}0}$ (E_0) and crystallinity (x_c) (all deduced from fitting absorption spectra based on the Franck-Condon equation (m = 2)), the enthalpy of fusion and the melting temperature of P3HT films crystallized at different conditions (see Experimental details section). The samples isothermally crystallized at T_c have been examined after subsequent quenching to room temperature. The enthalpy of fusion and the melting temperature were obtained by DSC from bulk P3HT samples with a mass of 4 mg. All other quantities were obtained by UV–vis spectroscopy of spin-coated P3HT films having a mass in order of a few μg.

resulting from quenching the sample from T_c to room temperature, was lost before reaching the peak of melting curve. In other words, the melting peak in the DSC curves resulted (mainly) from crystals created at T_c and was not affected by crystalline order induced upon quenching the sample.

3.1.4. Comparing the characteristics of the semicrystalline structure of differently crystallized P3HT films at room temperature

The crystallinity and crystalline quality of different isothermally and non-isothermally crystallized P3HT films are compared in Fig. 6 (and Appendix A (Table 1)). The isothermally crystallized films were examined after quenching to room temperature. In spite of the similar crystallinity for all the films, the lowest values of σ (≈73 meV) and W (≈70 meV) were found for the P3HT film, which was slowly cooled (at a rate of 1 °C/min) directly from the melt at 260 °C down to room temperature. A lower value of W corresponds to a higher conjugation length and higher intrachain order exhibiting higher quality of the order within the crystalline regions of the slowly cooled film. Correspondingly, a higher $A_{0\text{-}0}/A_{0\text{-}1}$ ratio was recorded for this sample (Appendix A (Table 1) and Appendix D (Fig. 12)). However, we also observed that employing higher crystallization temperatures allowed improving the crystalline quality. For the slowly cooled P3HT film and those crystallized for 4 h at 216 and 225 °C, similar values of σ and W were recorded. At higher crystallization temperatures, the rate of polymer crystallization was slower, providing more time for ordering polymer chains more perfectly at the crystal growth front.

The lowest enthalpy of fusion was recorded for the T_c216 sample. Before the measurement, all isothermally crystallized samples were quenched to room temperature. Thus, we expect to observe comparable values of crystallinity and enthalpy of fusion for these samples. We have no explanation for the obvious difference in enthalpy of fusion of the T_c216 sample. Rapid cooling from the melt to room temperature created thinner lamellar crystals which exhibited a lower melting temperature (in case of the rapidly cooled sample) while thicker crystals with a higher melting temperature were grown at a high isothermal crystallization temperature, e.g., at T_c = 216 °C.

Subsequent to the characterization by UV–vis spectroscopy, we examined all P3HT films discussed in Fig. 6 by atomic force microscopy. Although all P3HT films exhibited similar crystallinities (see Fig. 6), the as-cast and the rapidly cooled films (Fig. 7 (a, b)), comparing to the other films (Fig. 7 (c, d)), did not show a well-defined lamellar structure with a periodicity related to the alternation of crystalline and amorphous zones. These films were crystallized rapidly either during evaporating the solvent in the course of spin-coating or during cooling at a rate of around 100 °C/min from the melt to room temperature, respectively. Regarding to the chains arrangement in the crystallites relative to the substrate, the b-c plane is observed in the AFM images, showing the lamellar thickness (or crystal thickness in the chain direction) [2,37]. The resolution of the AFM images did not allow to extract precise values of the lamellar thickness. We observed mean value of the lamellar thickness around 14 nm with a variance of ±7 nm.

3.2. Crystalline features of P3HT bulk samples deduced from the analysis of WAXS/SAXS spectra

In contrast to UV–vis spectroscopy measurements, X-ray diffraction experiments were carried out on P3HT bulk samples. Appendix E presents WAXS pattern and Lorentz-corrected SAXS pattern along with the corresponding one-dimensional correlation function for the slowly cooled P3HT sample. The Bragg peaks indicated in Appendix E (Fig. 13 (a)) are consistent with the typical pattern reported for P3HT [37,38]. The (100) reflection peak, at $2\theta = 5.3°$, and the (020) reflection peak, at $2\theta = 23.6°$, are associated with π-stacked polythiophene backbones separated by 3-hexyl side chains (with a period of $d_{100} = 1.67$ nm in the a-direction) and the π-stacking distance between two chains of $d_{020} = 0.38$ nm (in the b-direction), respectively (Appendix E (Table 4)) [2].

We obtained crystallinity values $x_c \approx 0.6$, similar for all variously crystallized P3HT samples. However, these values derived from X-ray experiments were higher than the values of around $x_c \approx 0.4$, obtained from absorption spectra of similarly crystallized P3HT films, as reported in Appendix A (Table 3). This difference in crystallinity values may result from the different evaluation methods applied for the determination of crystallinity and may also be due to different methods of sample preparation, as discussed above in the context of the DSC curves in Fig. 3.

In comparison to the other samples, the narrower (100) Bragg peak for the slowly cooled P3HT sample (with a smaller full width at half maximum (FWHM), as shown in Appendix E (Table 4)) revealed the higher quality of order (the lower fraction of defects) in the crystalline regions of this sample. A similar crystalline quality was obtained when performing crystallization at high temperatures (e.g., at T_c = 216 °C for the T_c216). This observation is in full agreement with the results derived from the P3HT films shown in Fig. 6 (and Appendix A (Table 1)). The coherent size (ξ) of the crystallites was estimated in a- and b-directions by applying the Scherrer equation for the (100) and (020) Bragg peaks (see Appendix E), suggesting the presence of larger crystallites in the slowly cooled P3HT sample and in ones isothermally crystallized at high

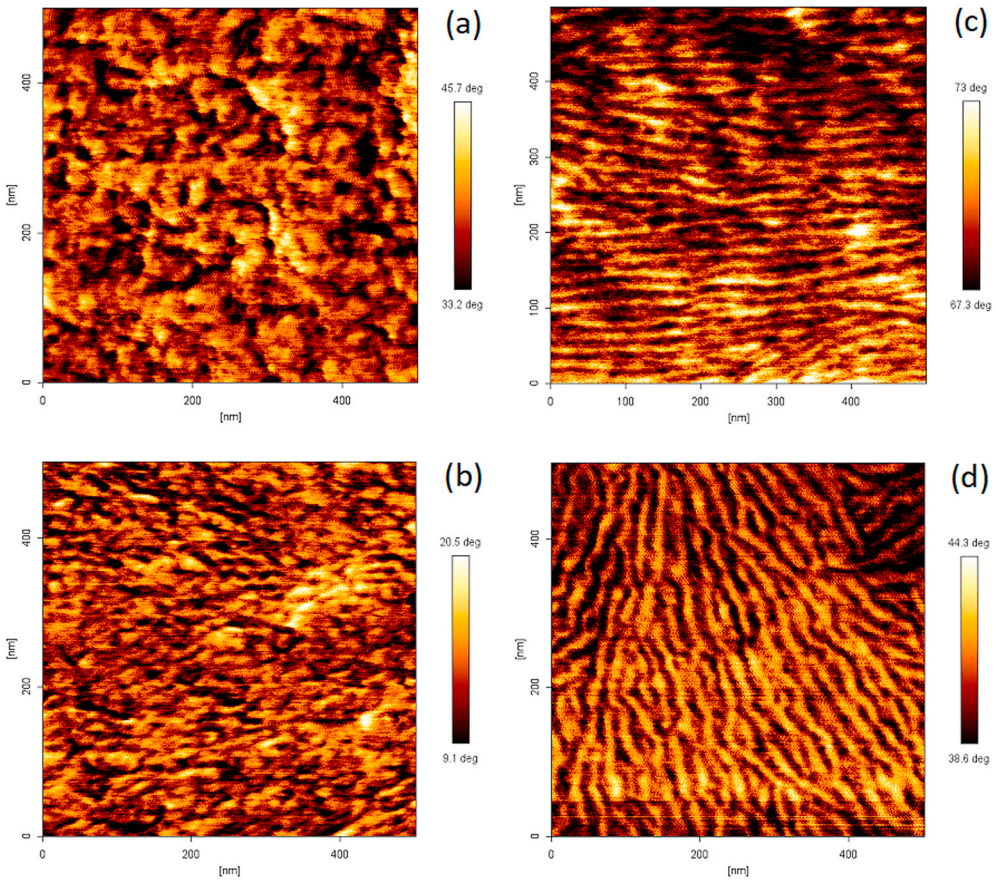

Fig. 7. Tapping mode AFM phase images taken on (a) as-cast, (b) rapidly cooled, (c) slowly cooled films and (d) the film isothermally crystallized for 4 h at 216 °C with subsequent quenching to room temperature.

T_c.

The maximum in the Lorentz-corrected SAXS pattern (Appendix E (Fig. 13 (b))) is associated with a periodic structure related to the alternation of crystalline and amorphous zones. From the one-dimensional correlation function (Appendix E (Fig. 13 (c))), the long period (L_p) and two lengths L_1 and L_2 corresponding to the thicknesses of the ordered and the amorphous phases were derived. Intriguingly, we observed that the values recorded for L_2 (from SAXS) (Appendix E (Table 4)) were comparable with the values of the conjugation length deduced from the UV–vis spectra (Appendix A (Table 1)). The values of L_2 were also consistent with the lamellar thickness deduced from the AFM images (Fig. 7). These observations may allow one to associate L_2 with the lamellar thickness (or crystal size in the chain direction, *i.e* in (001) direction). Nevertheless, regarding to our current results and previously published reports [15,31], as different methods for crystallinity evaluation of P3HT have led to different values for the same sample, whether L_1 or L_2 is the lamellar thickness, remains an open question for the meantime.

3.3. Solution-grown P3HT nanofibers versus melt-grown P3HT crystals

After a thorough investigation of P3HT crystals from the melt, we can come up with the P3HT crystals grown from the solution widely studied in the literature [3,16,18,22–29]. Due to π-π interactions between their rigid thienyl backbones, dissolved P3HT molecules tend to self-assemble into one-dimensional nanofibers when the solubility is reduced by temperature, addition of a nonsolvent, or evaporation [39]. We crystallized P3HT as nanofibers from its solution in a good solvent, toluene and a poor solvent, 3-hexylthiophene, simply by lowering the temperature below the dissolution temperature. Fig. 8 presents the AFM phase images of these nanofibers which were spin-coated on silicon substrates. Due to a higher solubility of P3HT in toluene, even after several days keeping the solution at room temperature, only a low fraction of the P3HT chains aggregated to form as suspended nanofibers, while the others remained as dissolved individual chains. This was clear from the light brown color of the obtained solution and verified by a lower population of the P3HT nanofibers settled on the substrate (Fig. 8 (a)). The space between the nanofibers on the substrate was covered with the P3HT crystals formed from the dissolved chains during the spin coating process due to the solvent evaporation and would resemble the microstructure of the as cast films in Fig. 7 (a). However, a poorer solubility of P3HT in 3-hexylthiophene caused most of the P3HT chains form nanofibers upon cooling the solution down to room temperature. A higher density of the nanofibers on the substrate (Fig. 8 (b)) was readily expectable, since the color of the solution was purple at room temperature.

It is already identified P3HT macromolecules are oriented perpendicular to the long axis of the nanofibers [40] and lie with their b-c plane on the substrate [41]. Consequently, as for P3HT crystals grown from the melt (Fig. 7), the width of the nanofibers in AFM phase images represents their lamellar thickness. Nanofibers prepared from both toluene and 3-hexylthiophene solutions showed an average width (or lamellar thickness) of around 30 nm which is about two times the lamellar thickness we observed for the melt-grown crystals (Fig. 7). It would be interesting to investigate how this significant difference in the lamellar thickness presents itself in the thermal and scattering characteristics of these crystals. Would it result in crystallinity and crystalline quality superior to those of melt-grown crystals? Our next work is meant to clarify the issue.

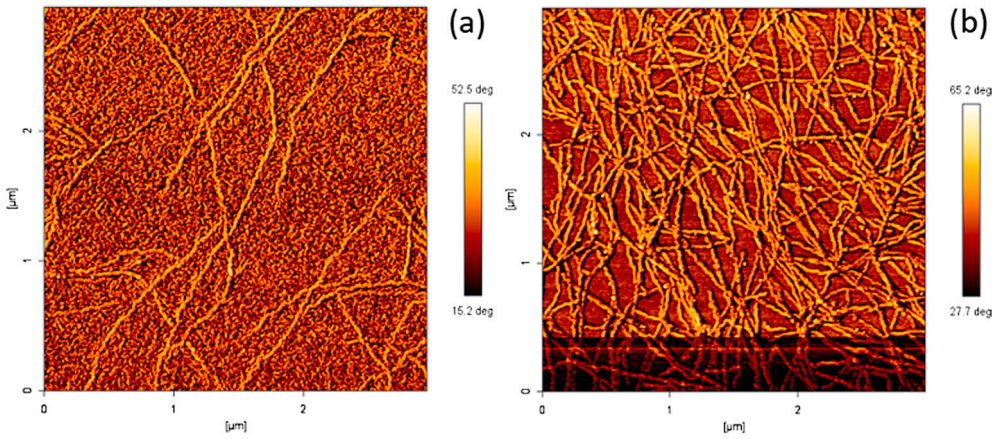

Fig. 8. Tapping mode AFM phase images taken on the nanofibers grown from P3HT solution in (a) toluene and (b) 3-heylthiophene.

4. Conclusions

UV–vis absorption spectroscopy combined with a Franck-Condon analysis was applied to study crystallization of spin-coated P3HT films from the melt. The absorption spectra taken during the non-isothermal crystallization (slow and rapid cooling from the melt) and isothermal crystallization at different crystallization temperatures demonstrated the development of order in these films as a function of the temperature and time. The samples crystallized at lower temperatures showed higher crystallinity with lower quality of the order in the crystalline regions, when they were evaluated at their crystallization temperatures. Quality of the order in crystalline structures created by isothermal crystallization at high temperatures was comparable to the one created by cooling the sample slowly from the melt to room temperature. These findings from absorption measurements were supported by a similar width of the Bragg X-ray reflection peaks for these samples. While all crystallized films had similar crystallinities at room temperature, AFM phase images taken on as-cast spin-coated films and films crystallized by a rapid cooling from the melt to room temperature did not exhibit a well-developed lamellar structure. Furthermore, heating the P3HT film in the temperature range of 40–175 °C did not change the crystallinity of the film, while quality of the order decreased continuously. Therefore, a clear difference is verified between two apparently similar structural characteristics of a semicrystalline polymer, crystallinity and quality of the order within crystalline domains.

CRediT authorship contribution statement

Mina Alizadehaghdam: Conceptualization, Investigation, Formal analysis, Writing - original draft. **Barbara Heck:** Investigation, Formal analysis. **Silvia Siegenführ:** Resources. **Yaser A. AlShetwi:** Formal analysis. **Fanuel M. Keheze:** Formal analysis. **Sebastian Stäter:** Formal analysis. **Farhang Abbasi:** Supervision, Writing - review & editing. **Günter Reiter:** Supervision, Writing - review & editing.

Declaration of competing interest

The authors declare that they have no known competing financial interests or personal relationships that could have appeared to influence the work reported in this paper.

Acknowledgements

This research did not receive any specific grant from funding agencies in the public, commercial, or not-for-profit sectors.

Appendix A. Supplementary data

Supplementary data to this article can be found online at https://doi.org/10.1016/j.polymer.2020.122959.

References

[1] P. Willot, J. Steverlynck, D. Moerman, P. Leclère, R. Lazzaroni, G. Koeckelberghs, Poly(3-alkylthiophene) with tuneable regioregularity:synthesis and self-assembling properties, Polym. Chem. 4 (2013) 2662–2671.
[2] M. Brinkmann, Structure and morphology control in thin films of regioregular poly (3-hexylthiophene), J. Polym. Sci. B Polym. Phys. 49 (17) (2011) 1218–1233.
[3] N.E. Persson, P.-H. Chu, M. McBride, M. Grover, E. Reichmanis, Nucleation, growth, and alignment of poly(3-hexylthiophene) nanofibers for high-performance OFETs, Acc. Chem. Res. 50 (4) (2017) 932–942.
[4] A. Wadsworth, Z. Hamid, M. Bidwell, R.S. Ashraf, J.I. Khan, D.H. Anjum, C. Cendra, J. Yan, E. Rezasoltani, A.A.Y. Guilbert, M. Azzouzi, N. Gasparini, J. H. Bannock, D. Baran, H. Wu, J.C. de Mello, C.J. Brabec, A. Salleo, J. Nelson, F. Laquai, I. McCulloch, Progress in poly (3-hexylthiophene) organic solar cells and the influence of its molecular weight on device performance, Adv. Energy Mater. 8 (28) (2018) 1801001.
[5] Z.D. Seibers, T.P. Le, Y. Lee, E.D. Gomez, S.M. Kilbey, Impact of low molecular weight poly(3-hexylthiophene)s as additives in organic photovoltaic devices, ACS Appl. Mater. Interfaces 10 (3) (2018) 2752–2761.
[6] Q. Liang, X. Jiao, Y. Yan, Z. Xie, G. Lu, J. Liu, Y. Han, Separating crystallization process of P3HT and O-IDTBR to construct highly crystalline interpenetrating network with optimized vertical phase separation, Adv. Funct. Mater. 29 (2019) 1807591.
[7] D. Bhattacharyya, A. Montenegro, P. Dhar, M. Mammetkuliyev, R.M. Pankow, M. C. Jung, M.E. Thompson, B.C. Thompson, A.V. Benderskii, Molecular orientation of poly-3-hexylthiophene at the buried interface with fullerene, J. Phys. Chem. Lett. 10 (8) (2019) 1757–1762.
[8] E.H. Jung, N.J. Jeon, E.Y. Park, C.S. Moon, T.J. Shin, T.-Y. Yang, J.H. Noh, J. Seo, Efficient, stable and scalable perovskite solar cells using poly(3-hexylthiophene), Nature 567 (2019) 511–515.
[9] Z. Liang, M. Li, Q. Wang, Y. Qin, S.J. Stuard, Z. Peng, Y. Deng, H. Ade, L. Ye, Y. Geng, Optimization requirements of efficient polythiophene:nonfullerene organic solar cells, Joule 4 (6) (2020) 1278–1295.
[10] Y.-A. Su, N. Maebayashi, H. Fujita, Y.-C. Lin, C.-I. Chen, W.-C. Chen, T. Michinobu, C.-C. Chueh, T. Higashihara, Development of block copolymers with poly(3-hexylthiophene) segments as compatibilizers in non-fullerene organic solar cells, ACS Appl. Mater. Interfaces 10 (2020) 12083–12092.
[11] H.-C. Liao, C.-S. Tsao, Y.-C. Huang, M.-H. Jao, K.-Y. Tien, C.-M. Chuang, C.-Y. Chen, C.-J. Su, U.-S. Jeng, Y.-F. Chend, W.-F. Su, Insights into solvent vapor annealing on the performance of bulk heterojunction solar cells by a quantitative nanomorphology study, RSC Adv. 4 (2014) 6246–6253.
[12] L.H. Jimison, S. Himmelberger, D.T. Duong, J. Rivnay, M.F. Toney, A. Salleo, Vertical confinement and interface effects on the microstructure and charge transport of P3HT thin films, J. Polym. Sci. B Polym. Phys. 51 (7) (2013) 611–620.
[13] Y. Kim, J. Nelson, J.R. Durrant, D.D.C. Bradley, K. Heo, J. Park, H. Kim, I. McCulloch, M. Heeney, M. Ree, Polymer chain/nanocrystal ordering in thin films of regioregular poly (3-hexylthiophene) and blends with a soluble fullerene, Soft Matter 3 (1) (2007) 117–121.
[14] H. Yang, T. Joo Shin, Z. Bao, C.Y. Ryu, Structural transitions of nanocrystalline domains in regioregular poly (3-hexyl thiophene) thin films, J. Polym. Sci. B Polym. Phys. 45 (11) (2007) 1303–1312.
[15] X. Shen, W. Hu, T.P. Russell, Measuring the degree of crystallinity in semicrystalline regioregular poly(3-hexylthiophene), Macromolecules 49 (12) (2016) 4501–4509.

[16] Y. Yuan, J. Shu, P. Liu, Y. Zhang, Y. Duan, J. Zhang, Study on π-π interaction in H- and J-aggregates of poly(3-hexylthiophene) nanowires by multiple techniques, J. Phys. Chem. C 119 (26) (2015) 8446–8456.
[17] F.M. McFarland, B. Brickson, S. Guo, Layered poly(3-hexylthiophene) nanowhiskers studied by atomic force microscopy and kelvin probe force microscopy, Macromolecules 48 (9) (2015) 3049–3056.
[18] K. Rahimi, I. Botiz, N. Stingelin, N. Kayunkid, M. Sommer, F.P.V. Koch, H. Nguyen, O. Coulembier, P. Dubois, M. Brinkmann, G. Reiter, Controllable processes for generating large single crystals of poly (3-hexylthiophene), Angew. Chem. Int. Ed. 51 (44) (2012) 11131–11135.
[19] J. Balko, A. Rinscheid, A. Wurm, C. Schick, R.H. Lohwasser, M. Thelakkat, T. Thurn-Albrecht, Crystallinity of poly(3-hexylthiophene) in thin films determined by fast scanning calorimetry, J. Polym. Sci. Polym. Phys. Ed 54 (2016) 1791–1801.
[20] M. Reichenberger, S. Baderschneider, D. Kroh, S. Grauf, J. Köhler, R. Hildner, A. Köhler, Watching paint dry: the impact of diiodooctane on the kinetics of aggregate formation in thin films of poly(3-hexylthiophene), Macromolecules 49 (2016) 6420–6430.
[21] F.M. Keheze, D. Raithel, T. Wu, D. Schiefer, M. Sommer, R. Hildner, G. Reiter, Signatures of melting and recrystallization of a bulky substituted poly(thiophene) identified by optical spectroscopy, Macromolecules 50 (17) (2017) 6829–6839.
[22] J. Clark, J.-F. Chang, F.C. Spano, R.H. Friend, C.S. Silva, Determining exciton bandwidth and film microstructure in polythiophene films using linear absorption spectroscopy, Appl. Phys. Lett. 94 (2009) 163306.1–163306.3.
[23] J.D. Roehling, I. Arslan, A.J. Moule, Controlling microstructure in poly(3-hexylthiophene) nanofibers, J. Mater. Chem. 22 (2012) 2498–2506.
[24] S. Sun, T. Salim, L.H. Wong, Y.L. Foo, F. Boey, Y.M. Lam, A new insight into controlling poly(3-hexylthiophene) nanofiber growth through a mixed-solvent approach for organic photovoltaics applications, J. Mater. Chem. 21 (2011) 377–386.
[25] D. Choi, M. Chang, E. Reichmanis, Controlled assembly of poly(3-hexylthiophene): managing the disorder to order transition on the nano- through meso-scales, Adv. Funct. Mater. 25 (6) (2015) 920–927.
[26] C. Scharsich, R.H. Lohwasser, M. Sommer, U. Asawapirom, U. Scherf, M. Thelakkat, D. Neher, A. Köhler, Control of aggregate formation in poly(3-hexylthiophene) by solvent, molecular weight, and synthetic method, J. Polym. Sci. B Polym. Phys. 50 (2012) 442–453.
[27] X. Zhang, Y. Liu, X. Ma, H. Deng, Y. Zheng, F. Liu, J. Zhou, L. Li, H. Huo, Sonocrystallization of poly(3-hexylthiophene) in a marginal solvent, Soft Matter 14 (18) (2018) 3590–3600.
[28] N. Kleinhenz, N. Persson, Z. Xue, P. Hsun Chu, G. Wang, Z. Yuan, M.A. McBride, D. Choi, M.A. Grover, E. Reichmanis, Ordering of poly(3-hexylthiophene) in solutions and films: effects of fiber length and grain boundaries on anisotropy and mobility, Chem. Mater. 28 (11) (2016) 3905–3913.
[29] K.A. Mazzio, A.H. Rice, M.M. Durban, C.K. Luscombe, Effect of regioregularity on charge transport and structural and excitonic coherence in poly(3-hexylthiophene) nanowires, J. Phys. Chem. C 119 (27) (2015) 14911–14918.
[30] A. Hamidi-Sakr, L. Biniek, S. Fall, M. Brinkmann, Precise control of lamellar thickness in highly oriented regioregular poly(3-hexylthiophene) thin films prepared by high-temperature rubbing: correlations with optical properties and charge transport, Adv. Funct. Mater. 26 (2016) 408–420.
[31] M. Alizadehaghdam, B. Heck, S. Siegenführ, F. Abbasi, G. Reiter, Thermodynamic features of perfectly crystalline poly(3-hexylthiophene) revealed through studies of imperfect crystals, Macromolecules 52 (6) (2019) 2487–2494.
[32] M. Alizadehaghdam, S. Siegenführ, F. Abbasi, G. Reiter, Thermodynamic features of perfectly crystalline poly(3-hexylthiophene) based on flory's relation, J. Polym. Sci. B Polym. Phys. 57 (2019) 431–437.
[33] G. Strobl, A new method for evaluating slit-smeared small angle X-ray scattering data, Acta Crystallogr. 26 (1970) 367–375.
[34] K. Rahimi, PhD thesis: controlling the crystal growth and morphology of conjugated polymers. Fakultät für Mathematik und Physik, Albert-Ludwigs-Universität Freiburg, 2013.
[35] F. Panzer, M. Sommer, H. Bässler, M. Thelakkat, A. Köhler, Spectroscopic signature of two distinct H-aggregate species in poly(3-hexylthiophene), Macromolecules 48 (5) (2015) 1543–1553.
[36] P. Kohn, S. Huettner, H. Komber, V. Senkovskyy, R. Tkachov, A. Kiriy, R.H. Friend, U. Steiner, W.T.S. Huck, J.-U. Sommer, On the role of single regiodefects and polydispersity in regioregular poly (3-hexylthiophene): defect distribution, synthesis of defect-free chains, and a simple model for the determination of crystallinity, J. Am. Chem. Soc. 134 (10) (2012) 4790–4805.
[37] Z. Wu, A. Petzold, T. Henze, T. Thurn-Albrecht, R.H. Lohwasser, M. Sommer, M. Thelakkat, Temperature and molecular weight dependent hierarchical equilibrium structures in semiconducting poly (3-hexylthiophene), Macromolecules 43 (10) (2010) 4646–4653.
[38] A. Zen, M. Saphiannikova, D. Neher, J.r. Grenzer, S. Grigorian, U. Pietsch, U. Asawapirom, S. Janietz, U. Scherf, I. Lieberwirth, Effect of molecular weight on the structure and crystallinity of poly (3-hexylthiophene), Macromolecules 39 (6) (2006) 2162–2171.
[39] G. Yan, H. Yuanyuan, Su Zhaohui, Ordering of poly(3-hexylthiophene) in solution and on substrates induced by concentrated sulfuric acid, J. Phys. Chem. B 117 (47) (2013) 14842–14848.
[40] I. Kyo Jin, M. Jeff, S. Paul, Whiskers of poly (3-alkylthiophene)s, J. Polym. Sci. B Polym. Phys. 31 (6) (1993) 735–742.
[41] H. Yuanyuan, G. Yan, C. Yingfei, G. Yanhou, S. Zhaohui, Chain folding in poly (3-hexylthiophene) crystals, Macromolecules 47 (11) (2014) 3708–3712.